Journal of Applied Electrochemistry **33**: 909–915, 2003.

Effect of crystal structure on the electrochemical behaviour of synthetic semiconductor diamond: Comparison of growth and a nucleation surfaces of a coarse-grained polycrystalline film☆

Yu.V. PLESKOV[1,*], Yu.E. EVSTEFEEVA[1], M.D. KROTOVA[1], V.G. RALCHENKO[2], I.I. VLASOV[2], E.N. LOUBNIN[3] and A.V. KHOMICH[4]
[1]*Frumkin Institute of Electrochemistry, Russian Academy of Sciences, 119071 Moscow, Russia*
[2]*General Physics Institute RAS, 38 Vavilova Street, 117942 Moscow, Russia*
[3]*Institute of Physical Chemistry RAS, 31 Leninsky prospekt, 117915 Moscow, Russia*
[4]*Institute of Radio Engineering and Electronics RAS, 1 Vvedenskogo square, 141190 Fryazino, Russia*
*(*author for correspondence, e-mail: pleskov@electrochem.msk.ru)*

Received 10 October 2002; accepted in revised form 28 May 2003

Key words: acceptor, boron-doped diamond, crystallite, electrochemical impedance, thin-film electrode

Abstract

Comparative studies of the electrochemical behaviour of the growth and nucleation surfaces of a free-standing boron-doped polycrystalline diamond film grown in a microwave plasma CVD reactor are performed. The uncompensated acceptor concentration in diamond is determined from the electrochemical impedance (Mott–Schottky plots), uncompensated boron acceptor concentration from infrared absorption measurements, and the total boron concentration, by the SIMS method. In the diamond bulk adjacent to the nucleation surface, constituted from submicrometre-sized crystallites, both the boron concentration and the total acceptor concentration are found to be significantly higher than near the growth surface, where the film crystallinity is more perfect. This difference is tentatively attributed to the increased concentration of crystal lattice defects near the nucleation surface. These defects, in addition to boron atoms, play the role of acceptors in diamond.

1. Introduction

Effects of crystal structure of solids on their electrochemical behaviour are well known in the electrochemistry of semiconductors [1]. In particular, structural defects (e.g., emerging during mechanical processing) manifest themselves in the electronic spectrum as surface or bulk states affecting transport, kinetic and other properties of solids; the adsorption capacity of different faces of a crystal can depend on surface atomic density.

As applied to diamond electrodes, the interrelation between their crystal structure and electrochemical behaviour was touched upon in comparative studies of CVD polycrystalline and single crystal thin-film electrodes and HTHP single crystal, as well as diamond-like carbon thin-film electrodes ([2] see references therein). Possible specific contribution of sp^2-carbon inclusions to electrochemical properties of polycrystalline diamond is widely discussed in the literature. It was shown [3] that the electrical double-layer structures on electrodes of single crystal and polycrystalline diamond is similar, on the whole. Comparative studies of the kinetics of electrochemical reactions proceeding in numerous redox couples showed that single crystal and polycrystalline diamond electrodes are close to each other as regards their kinetic characteristics, at least, at moderate polarization. It was concluded [3] that intercrystallite boundaries, constituted by disordered carbon, contribute negligibly to the electrode behaviour of polycrystalline diamond, which is mainly determined by diamond crystallites proper. However, the intercrystallite boundaries sometimes manifest themselves in the shape of potentiodynamic curves [4]; this is a second order effect.

In this paper we compared electrochemical properties of two sides of a free-standing polycrystalline diamond film, namely, an outer (growth) side and an inner (nucleation) side. The growth side is rough because it is composed of the microcrystallite facets; the nucleation side, at which the diamond nucleation starts, is rather smooth being a replica of the mirror-polished silicon substrate. The growth diamond surface and its adjacent crystallites have a relatively perfect crystallinity; by contrast, the nucleation surface and its adjacent diamond bulk constituted by submicrometre-sized grains is believed to have an elevated concentration of both impurities, like Si, H [5, 6], and various structural

☆ This paper was originally presented at the 6th European Symposium on Electrochemical Engineering, Düsseldorf, Germany, September 2002.

defects. Recently, we performed such a comparative study on relatively thin (3 to 6 μm in thickness) films. We found that their two surfaces differ insignificantly in their impedance and kinetic characteristics [7]. This can be explained by the relative uniformity of thin films, as regards their defect structure, because they are fine-grained over their entire thickness. To reveal possible effect of the crystal structure on the electrode behaviour of the growth and nucleation surfaces of CVD films, we now chose a much thicker (400 μm thick) film for which we expected that the difference in the crystallinity of the two sides has been well developed.

2. Experimental details

2.1. *Samples preparation*

A 0.4 mm thick polycrystalline diamond wafer was deposited from a methane(2%)–hydrogen(98%) mixture activated by a 5 kW microwave discharge; the procedure is described in detail in [8]. A polished single-crystal silicon plate (62 mm dia. × 3 mm thick) was the substrate. During the deposition, it was heated by plasma to 690 °C. Diamond was doped with boron, during the film growth, using the plasma sputtering (etching) of a graphite pellet impregnated with boron.

Upon etching-off the silicon substrate in a HF—HNO_3 mixture, the resulting free-standing diamond wafer was light blue, which is characteristic of moderately boron-doped diamond crystals. The samples were rectangular plates 1 cm × 1 cm, cut off from the wafer using a Cu-vapour laser. To remove the conducting graphitized layer that formed in the laser-cut area, the samples were annealed in air at 550 °C for 1 h.

For closer inspection of the layer adjacent to the nucleation surface, on completing the measurements performed at this surface, a 15 μm thick diamond layer was mechanically polished off on a scafe from this side, and the electrochemical and optical measurements were repeated at the newly formed surface.

The diamond structure is essentially nonuniform across the wafer: it is a columnar-crystallite system (typical of CVD diamond). At the smooth nucleation side, from where diamond originates, grains are very small (~100 nm according to AFM measurements) and randomly arranged. As a result of a directional grain selection during further growth, a {110}-directed texture is developed, as follows from X-ray diffraction patterns. The crystallites turn columnar; therefore, the rough growth surface acquires a faceted morphology, and with crystallite faces sized 10–60 μm. The surface roughness (r.m.s.) on the growth side was 3.4 μm as measured with a white light interference microscope (ZYGO).

2.2. *Optical measurements*

Raman spectra were taken using an S-3000 microprobe Raman spectrometer (ISA/Jobin Yvon), in a backscattering geometry; the scattering was excited with an Ar-laser line of 514 nm wavelength. A spatial resolution of 2 μm in diameter and 5 μm in depth was achieved using a confocal optical scheme. The spectra were recorded with a 1.8 cm^{-1} spectral resolution matrix detector.

Optical transmission spectra were recorded using two-beam spectrophotometers: a Specord-M80, in the 2.5–50 μm range, and a Specord-M400, in the 0.185 to 0.9 μm range. The absorption coefficient α was obtained using the following equation: $\alpha = (1/d)\ln(T_o/T_{sample})$, where d is the film thickness, $T_o = 2n/(n^2+1)$ is the transmittance losses due to reflection from the diamond surfaces, and T_{sample} is the transmittance of the polished diamond film.

2.3. *SIMS measurements*

The absolute boron concentration was measured by secondary ion mass spectrometry (SIMS) using a Cameca IMS3f instrument. Primary O_2^+ ions (energy 5.6 keV, current 1 μA, beam spot 50 μm) were used to obtain the flux of positive ions from the analysed sample. Intensities of masses 10(B), 11(B), 12(C) and 13(C) were analysed in the SIMS spectra. The distribution of boron concentration was traced to a depth of 40 nm (at plateau in the B depth profile) both on the nucleation and growth sides.

2.4. *Preparation of electrodes: electrochemical measurements*

The electrodes were rectangular plates, 1 cm × 1 cm. For electrochemical measurements, Ti/Au contacts 5 mm in diameter were evaporated onto the rear of the plate. The contacts and current connections were insulated with a layer of high-purity paraffin. The electrode working area was ~0.2 cm^2. A three-compartment glass electrochemical cell was used. A normal Ag/AgCl electrode was the reference electrode (in what follows, all potential values are given against this electrode); the auxiliary electrode was made of platinum. Electrochemical measurements were performed in a well-conducting indifferent electrolyte solution (2.5 M H_2SO_4).

The electrode differential capacitance was measured using an R-5021 a.c. bridge (in a 20 Hz to 200 kHz frequency range) or a Solartron (model 1250) frequency analyser equipped with a model 1286 electrochemical-measuring unit (in a 0.1 Hz to 100 kHz frequency range). The equivalent circuit was calculated using the software described in [9].

3. Results

3.1. *Characterization*

3.1.1. *Optical spectroscopy*

In the Raman spectra recorded at both the growth and the nucleation sides (Figure 1), we see only a narrow

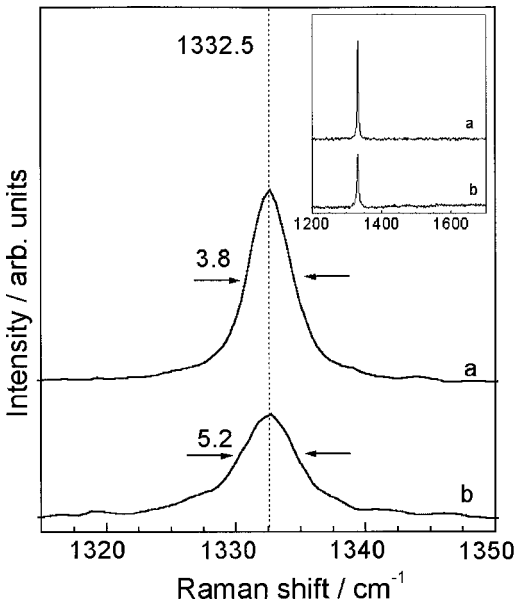

Fig. 1. Raman spectra for (a) growth side and (b) nucleation side of the diamond film, recorded at a high resolution near 1332 cm^{-1}. Insert: the same spectra presented in a wider frequency range, showing the absence of nondiamond carbon phases.

peak at 1332 cm^{-1}, indicating a sufficiently perfect diamond structure. No admixture of nondiamond phases (e.g., amorphous carbon, graphite), that would manifest themselves in the Raman spectra as characteristic maxima at higher frequencies was detected. However, the 1332 cm^{-1}-peak width (FWHM) is markedly larger at the fine-grained nucleation side (5.2 cm^{-1}) than that at the coarse-grained growth side (3.8 cm^{-1}), evidently, because of higher structure imperfection of the diamond in a thin layer formed during the initial stages of synthesis.

In infrared absorption spectra of the film (Figure 2) we observed, in addition to the intrinsic diamond two-phonon absorption near 2000 cm^{-1} and low-intensity CH_x-stretching bands (the concentration of bonded hydrogen in these sample is $N_{CH} = 150$ ppm), a series of

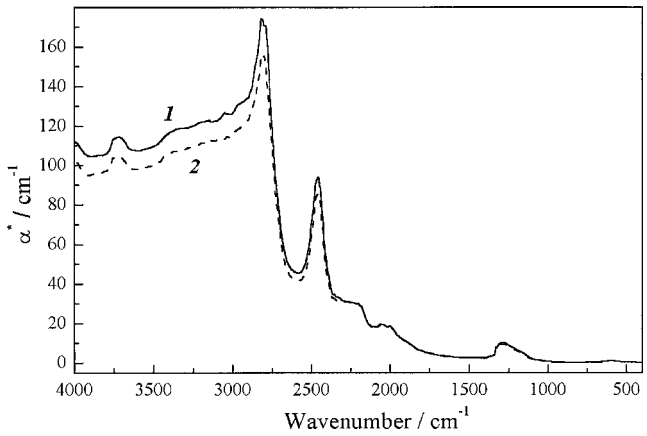

Fig. 2. Transmission spectrum of the diamond film (1) prior to and (2) upon polishing off a 15 μm thick layer at the nucleation side.

prominent zero-phonon lines in the 2400–4000 cm^{-1} range and the one phonon peak at 1290 cm^{-1} (normally this process is forbidden in diamond by selection rules but it is activated by the presence of the boron acceptors because the inversion symmetry of the lattice is broken), which are characteristic of the type IIb diamond. The peaks at 2460 cm^{-1} (0.304 eV), 2810 cm^{-1} (0.348 eV) and wide band at 2900–3000 cm^{-1} (0.36 eV) are due to electronic transitions for the boron acceptor: they correspond to the first, second, and third excited state transitions, respectively. A phonon side band is also observed at 3730 cm^{-1} (0.46 eV), which is associated with the first excited state of the boron impurity. These electronic transitions for the boron acceptor take positions characteristic of single crystal diamond; however, the lines are somewhat broadened, due to the polycrystalline nature of the CVD diamond film. These bands are superimposed at the photoionization continuum (background) extending from the infrared into the visible part of the spectrum to about 500 nm and producing the blue coloration characteristic of moderately and heavily boron-doped diamond.

The concentration of uncompensated acceptors in diamonds was calculated to an accuracy of 20% by the formula [10]

$$(N_A - N_D) = 4.45 \times 10^{-3} I_{0.348\,eV} \quad (1)$$

where $(N_A - N_D)$ is in ppm; $I_{0.348\ eV}$ (meV cm^{-1}) is the integrated area of the 0.348 eV (2810 cm^{-1}) peak, above the background curve; N_D is the donor (e.g., nitrogen) concentration. After removing a 15 μm thick layer from the nucleation side, the $N_B - N_D$ concentration averaged over the sample thickness decreased from 8.0×10^{17} cm^{-3} to 6.8×10^{17} cm^{-3}. This corresponds to a significantly higher value, $2.2 - 2.5 \times 10^{18}$ cm^{-3}, of the $N_B - N_D$ concentration averaged over the 'first' 15 μm thick layer at the nucleation side of the film (Table 1).

3.1.2. *SIMS*

The boron content in the diamond film was quantitatively determined by using, for calibration, two types of samples: (i) single crystal graphite impregnated with different B/C atomic ratios, from 5×10^{-4} to 9×10^{-3}, and (ii) CVD diamond implanted with ^{11}B ions with energy 120 keV and dose 1×10^{14} cm^{-2}. The B/C intensity ratio in the SIMS spectra for the graphite standards was found to depend linearly on the boron concentration up to about 10^{-2} at %, as shown in Figure 3(a). Therefore, we assumed that matrix effects, such as crystal structure or a solid solution formation, do not interfere with the quantification of the boron in the carbon matrix.

The SIMS spectrum taken at the polished growth side of the diamond film is shown in Figure 3(b). The intensity ratio of peaks 10 (B) and 11 (B) is close to that (0.23) known for natural abundance of boron isotopes ^{10}B and ^{11}B. No surface charging effects caused by the

Table 1. Comparison of data on the concentrations obtained by different techniques

Nucleation side		Averaged bulk		Growth side	Method	Measured value*
As grown	After 15 μm polished off	over first 15 μm at nucleation side	over the whole film thickness			
3×10^{18}	1.2×10^{18}			0.7×10^{17}	Impedance	$N_A - N_D$
9×10^{17}				1.5×10^{17}	C-V [11]	$N_A - N_D$
				0.55×10^{17}	Q-DLTS [11]	$N_B - N_D$
		2.4×10^{18}	8×10^{17}		IR absorption	$N_B - N_D$
$9(14) \times 10^{17}$				$0.2(0.3) \times 10^{17}$	SIMS	N_B

* N_B, N_A and N_D are the concentrations (per 1 cm^3) of boron, acceptors, and donors, respectively.

ion beam was observed, because of sufficiently high sample conductivity. Boron concentration of 9×10^{17} cm^{-3} on the nucleation side, and a value about 40 times lower, 0.2×10^{17} cm^{-3}, on the growth side were found with calibration based on graphite standard. However, calibration with ion-implanted diamond resulted in the higher, by a factor 1.6, boron concentrations, which are given in parenthesis in Table 1.

3.2. *Electrochemical impedance measurements*

The studied electrodes showed low background currents that did not interfere with the impedance measurements. The background current at the growth side was about 0.1 μA cm^{-2} over the -0.5 to $+1.5$ V potential range; on the nucleation side, the potential window was somewhat narrower.

Figure 4(a) shows impedance spectra for the growth side (curve 1) and the nucleation side (curve 2). Over a wide frequency range, the curves are semicircles (somewhat depressed), which can be approximated by the Randles equivalent circuit. The high frequency portion of the spectrum is an inclined straight line (Figure 4(b)); this type of frequency dispersion would be simulated by a constant phase element (CPE) in the equivalent circuit. The CPE impedance is

$$Z_{CPE} = \sigma^{-1}(i\omega)^{-a} \qquad (2)$$

where $i = (-1)^{1/2}$, $\omega = 2\pi f$ is the a.c. angular frequency (f is the measured a.c. frequency); and the frequency-independent factor σ is measured in $F^a\Omega^{a-1}$ cm^{-2} units. The CPE thus replaces a frequency-independent capacitance in the Randles circuit (Figure 4(c)).

The power a, which characterizes the frequency dispersion of impedance, is in the range 0.95–0.97 for both the growth and the nucleation sides. This value is close to unity; in other words, the frequency dispersion of the capacitance is relatively weak. In earlier studies of fine-grained polycrystalline diamond electrodes, we often obtained somewhat lower a values, specifically, 0.9 to 0.95 [3].

The 'capacitance' σ at the growth side was rather low ($\sim$0.003 $F^a\Omega^{a-1}$ cm^{-2}), as expected for a relatively lightly doped semiconductor. Assuming the roughness factor for the growth surface with a faceted morphology to be about 2.5, we obtained a value for σ of about 0.001 $F^a\Omega^{a-1}$ per unit true surface. (The 2.5 value is intermediate between theoretical estimates of 1.73 and 3.60 for an octahedron-edged and a cube-edged surface. Octahedron and cube are principal forms inherent in the surface morphology of diamond. This is the lower limit-estimate, indeed, because here the octahedron and cube faces are assumed being smooth. Actually, they contain growth steps of different size, which may increase the

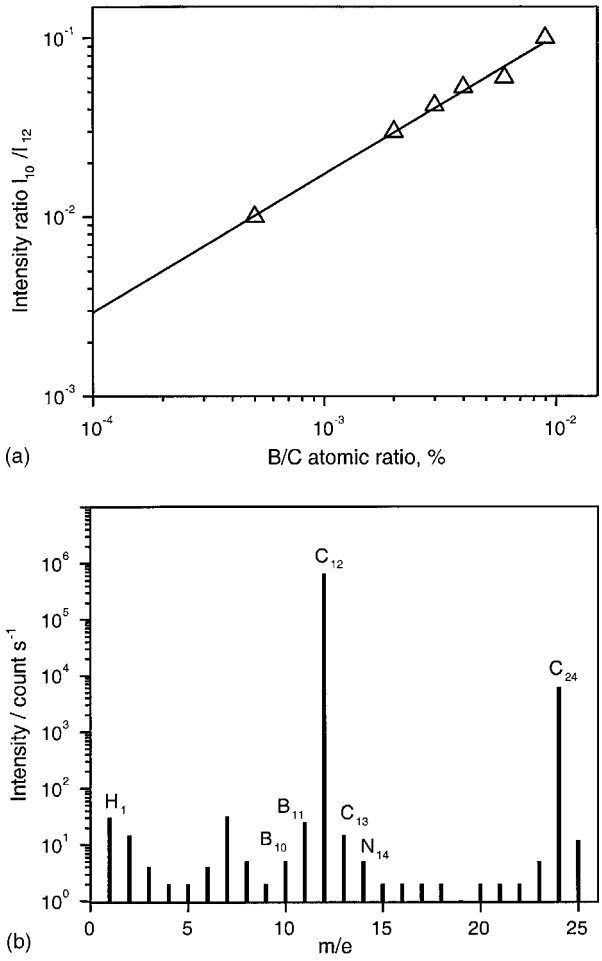

Fig. 3. (a) The B/C intensity ratio in the SIMS spectra taken at single crystal graphite samples impregnated with boron at different concentrations, used for spectra calibration; (b) a SIMS spectrum taken at the growth side of the diamond film.

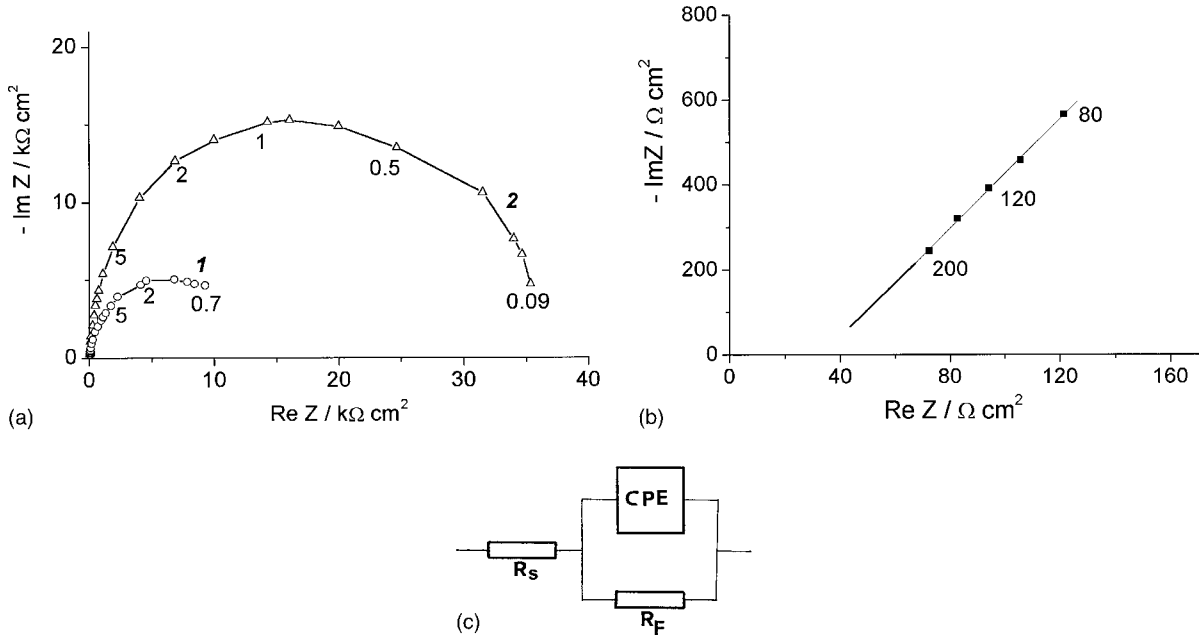

Fig. 4. (a) Impedance spectra for (1) the growth surface and (2) the nucleation surface of the diamond film; (b) the high-frequency portion of curve 1 for the growth surface; a.c. frequency values are shown next to the graphs; (c) equivalent circuit for the electrode: R_s is the diamond film bulk resistance; R_F is the faradaic resistance; and CPE is the constant phase element.

true surface area significantly.) At the nucleation side, the σ value is much higher.

From the series resistance R_s, we found the diamond film resistivity $\rho \sim 10^3\ \Omega$ cm. This value practically coincides with that obtained [11] for a similar sample from the impedance measured for a solid-state structure containing a diamond film/nickel junction. (The Ni contact to diamond, like the electrolytic contact we used, shows a Schottky diode behaviour.) The reliability of the ρ value was corroborated in [11] by independent measurements of the hole concentration ($p = 1.5 \times 10^{14}$ cm^{-3}) and hole mobility ($\mu_p = 35$ cm^2 V^{-1} s^{-1}), using the Hall effect method.

To determine the acceptor concentration in the diamond film, we used Mott–Schottky plots. In view of the aforementioned frequency dependence, this determination obviously gives only an estimate. We put $\boldsymbol{a} = 1$; in other words, we substituted a frequency-independent capacitance C for the CPE in the equivalent circuit of Figure 4(c). This capacitance was calculated using the least-squares method, by minimizing the root mean square deviation of the logarithm of the impedance modulus measured experimentally at different frequencies from that calculated for the chosen equivalent circuit [12]. The capacitance was thus 'averaged' over the whole frequency range (in the plots of Figure 5, from 630 Hz to 63 kHz). The C values were used in plotting Mott–Schottky lines. In Figure 5(a) is a Mott–Schottky plot for the growth side and likewise in Figure 5(b) for the nucleation side (after polishing off 15 μm). Both are straight lines, whose extrapolation to the potential axis gives flat-band potentials of 1.6 and 2.1 V, respectively. Such positive values point to a well oxidised state of the diamond surface [13], which is no surprise, since the film had been initially etched in an oxidizing bath and then annealed in air. The difference in the above values (~0.5 V) may reflect the difference in the oxidation state of the two surfaces. (Whether or not the polishing affected the flat-band potential of the nucleation surface still is an open question.)

From the slope of this straight line, using the well-known Schottky formula, we determined the concentration of uncompensated acceptors, $N_A - N_D = 4.1 \times 10^{17}$ cm^{-3}. With due allowance for the surface roughness (see above), we eventually come to a 'true' value of $N_A - N_D = 0.7 \times 10^{17}$ cm^{-3}. For the nucleation side, both as grown and polished, no correction for the roughness was introduced, because the nucleation surface is mirror-smooth (the roughness is less than 10 nm according to AFM data).

4. Discussion

All $N_A - N_D$ values obtained using different techniques are collected in Table 1. Additionally, we included the data found in [11] for samples cut from the same wafer, by using voltage against capacitance curves (similar to the above-shown Mott–Schottky plots) taken for the aforementioned diamond/Ni junction. Also, the data obtained by charge-based deep level transient spectroscopy (Q-DLTS) are included.

Analysis of the data, with due reservation for some experimental scatter, enables us to draw the following conclusions:

(i) The SIMS data (and, as indirect evidence, the impedance measurements) demonstrate a significant difference in the boron concentration, N_B, between the

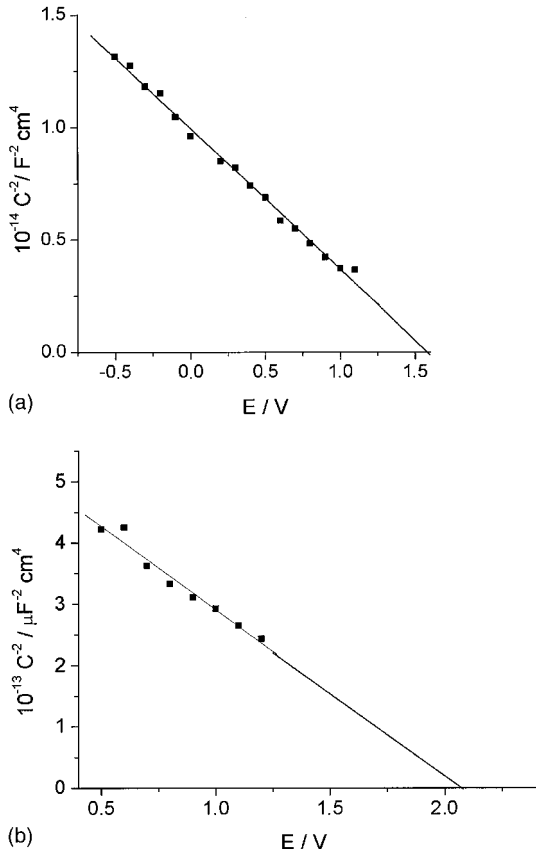

Fig. 5. Mott–Schottky plot for (a) the growth surface and (b) the nucleation surface after polishing off a 15 μm thick layer.

growth and nucleation sides of the film. This may be partly due to gradually decreasing dopant concentration in the source gas. Another possible reason is a partial segregation of boron atoms at intercrystallite boundaries and crystal lattice defects. Because of the fine-grained nature of the initial portions in growing diamond film, the 'weight' of the intercrystallite boundaries, which are capable of accommodating boron, is relatively large. Therefore, we have every reason to speculate that the diamond layer adjoining the nucleation side of the film is enriched in boron.

However, more probably the difference in the B concentration at the two sides of the film can be related to a growth-sector-orientation dependence of the intensity of boron incorporation in the diamond crystals. Boron is known to incorporate into {111} growth sectors up to 100 times more abundantly than into {100} growth sectors [14]. The incorporation of boron into various growth sectors was shown to decrease in the sequence {111} > {110} > {100} = {113} > {115} for HPHT diamond [15]. The X-ray diffraction analysis revealed a strong {110} texture of the sample growth surface; whereas the (111) peak was absent in the X-ray diffraction spectrum. However, because of random orientation of fine crystallites at the nucleation side, the {111} and {110} orientations are of comparable abundance, so the average boron concentration could be higher there, due to the presence of boron-enriched sectors.

(ii) The uncompensated acceptor concentration $N_A - N_D$ at the growth side, measured by the electrochemical method, approached that found from the voltage against capacitance curves taken for diamond/Ni junction [11]. (The difference by a factor of 2 might be thought of as insignificant because the true surface area was estimated with low accuracy, due to the unknown effective surface factor.) Thus, the impedance measurements for a diamond/metal rectifying junction and those for a blocking electrolytic contact are in reasonable agreement.

(iii) The $N_A - N_D$ concentration measured by the electrical methods for both the growth and nucleation sides turned out to be several times higher than the boron concentration N_B derived from the SIMS measurements. Thus tentatively, we suggest that some structural defects contribute, in addition to boron atoms, to the total acceptor concentration. Whether these defects are directly boron-induced, or boron merely reveals some inherent structural defects, we cannot distinguish at this stage. It is noteworthy that thick undoped films deposited in the same microwave CVD reactor are insulating (with the 10^{13} to 10^{14} Ω cm resistivity).

(iv) The total concentration of uncompensated acceptors, as evidenced by the impedance measurements, at the nucleation side is several times higher than that at the growth side. (We note that the $N_B - N_D$ value determined by infrared absorption is naturally averaged over the film thickness and, thus, falls between the two values found from the Mott–Schottky plots and related to thin, about 10^{-5} cm thick, layers adjacent to the film surfaces.) The elevated $N_A - N_D$ concentration at the nucleation side is only partly caused by the above-discussed enrichment in boron. Another reason is the imperfect crystal structure of the thin diamond layer formed in the initial stages of film growth. Hydrogen-related defects in the near-surface layer of hydrogenated diamond were proposed [16] to form shallow (0.03–1 eV) centres, and play the role of acceptors. However, our samples were oxidized prior to the measurements; thus other defects (potential acceptors) could be also considered. The depth profile of acceptor concentration was not measured; however it seems to be smooth, as no abrupt rise in the $N_A - N_D$ value is observed for the 15 μm thick layer at the nucleation side, as evidenced by the impedance and optical data (Table 1).

Hydrogen-boron interaction in highly boron-doped diamond (see, e.g., [17]) might be thought of as a further reason for the uneven boron concentration in the film. Due to midgap-donor behaviour of hydrogen in diamond, boron atoms become negatively charged upon hydrogen incorporation. However, we observed no evidence of B–H pair formation in the electrodes under study. The samples cut from the same diamond wafer were annealed in steps at temperatures between 850 and 1600 °C in a vacuum of 10^{-5} torr for 1 h. The boron-induced bands in the infrared spectra did not change upon annealing [18]: the corresponding change in the

uncompensated acceptor concentration $N_A - N_D$, calculated from the infrared spectra, was as small as 0.1 ppm. This finding seems to rule out the possibility of the presence of the B–H pairs in the untreated as-grown film, because these pairs are unstable at temperatures higher than 690 °C.

(v) We can judge the reactivity of the electrode by its faradaic resistance R_F, a value inversely proportional to the exchange current, which characterises the electrode reaction rate [19]. In Figure 4(a) we compared impedance spectra for the growth and nucleation sides, taken in the indifferent electrolyte solution. We see that the R_F value at the growth side (curve 1) is several times lower (that is, the reactivity is higher) than that at the nucleation side (curve 2). In the absence of deliberately added redox electrolyte, only traces of occasional impurities in the electrolyte or species in the adsorption layer can contribute to the current (the background current). Nonetheless, we may speculate that the growth surface, with its more perfect crystallinity, must be superior to the nucleation surface as regards its electrode characteristics.

5. Conclusions

The results obtained suggest that measuring the impedance of the diamond–electrolyte interface is a nondestructive method, which may be useful for determining bulk properties of diamond films [20]. The acceptor concentration in the coarse-grained diamond film was to be lower in the layer adjacent to its more perfect growth side than near the more defective nucleation side. In this respect the coarse-grained films differ from the fine-grained films studied earlier [5], which are evidently imperfect over their entire bulk. These features of crystal structure undoubtedly affect the electrochemical kinetics at diamond electrodes.

Acknowledgements

This work was supported in part by the Russian Foundation for Basic Research, projects 01-03-32 045 and 03-03-32396, the NEDO International Joint Research Grant Program (project 01MB9) and INTAS grant 01-2173. V.A. Dravin and R. Khmelnitsky are acknowledged for performing the ion implantation and V. Kononenko for surface roughness measurements.

References

1. Yu.V. Pleskov and Yu.Ya. Gurevich, 'Semiconductor Photoelectrochemistry' (New York, Consultants Bureau, 1986).
2. Yu.V. Pleskov, *Russ. Chem. Rev.* **68** (1999) 381.
3. Yu.E. Evstefeeva, M.D. Krotova, Yu.V. Pleskov, V.V. Elkin, V.P. Varnin and I.G. Teremetskaya, *Elektrokhimiya* **34** (1998) 1171.
4. H.B. Martin, A. Argoitia, U. Landau, A.B. Anderson and J.C. Angus, *J. Electrochem. Soc.* **143** (1996) L133.
5. L.C. Nistor, J. Van Landuyt, V.G. Ralchenko, E.D. Obraztsova and A.A. Smolin, *Diamond and Related Mater.* **6** (1997) 159.
6. V. Ralchenko, *in*: G. Benedek, P. Milani and V.G. Ralchenko (Eds), 'Nanostructured Carbon for Advanced Applications', (Kluwer, Dordrecht, 2001), p. 27.
7. Yu.V. Pleskov, M.D. Krotova, Yu.E. Evstefeeva, V.P. Varnin, I.G. Teremetskaya and V.I. Polyakov, *Elektrokhimiya* **37** (2001) 1299.
8. V. Ralchenko, I. Sychov, I. Vlasov, A. Vlasov, V. Konov, A. Khomich and S. Voronina, *Diamond and Related Mater.* **8** (1999) 189.
9. B.A. Boukamp, *Solid State Ionics* **20** (1986) 31.
10. A. Zaitsev, *in*: M.A. Prelas, G. Popovici and L.K. Bigelow (Eds), 'Handbook of Industrial Diamonds and Diamond Films' (Marcel Dekker, New York, 1997), p. 227.
11. V.I. Polyakov, A.I. Rukovishnikov, N.M. Rossukanyi and V.G. Ralchenko, *Diamond and Related Mater.* **10** (2001) 593.
12. Yu.E. Evstefeeva, M.D. Krotova, Yu.V. Pleskov, V.M. Mazin, V.V. Elkin, V.Ya. Mishuk, V.P. Varnin and I.G. Teremetskaya, *Elektrokhimiya* **34** (1998) 1493.
13. I. Yagi, H. Notsu, T. Kondo, D.A. Tryk and A. Fujishima, *J. Electroanal. Chem.* **473** (1999) 173.
14. R. Locher, J. Wagner, F. Fuchs, M. Maier, P. Gonon and P. Koidl, *Diamond and Related Mater.* **4** (1995) 678.
15. H. Kanda and T. Sekine, *in*: G. Davis (Ed.), 'Properties and Growth of Diamond' (INSPEC, The Institution of Electrical Engineers, London, 1994), p. 415.
16. O. Gaudin, M.D. Whitfield, J.S. Foord and R.B. Jackman, *Diamond and Related Mater.* **10** (2001) 610.
17. J. Chevallier, B. Theys, A. Lusson, C. Grattepain, A. Deneuville and E. Gheeraet, *Phys. Rev. B* **58** (1998) 7966.
18. A.V. Khomich, V.G. Ralchenko, A.V. Vlasov, R.A. Khmelnitskiy, I.I. Vlasov and V.I. Konov, *Diamond and Related Mater.* **10** (2001) 546.
19. A.D. Modestov, Yu.E. Evstefeeva, Yu.V. Pleskov, V.M. Mazin, V.P. Varnin and I.G. Teremetskaya, *J. Electroanal. Chem.* **431** (1997) 211.
20. Yu.V. Pleskov, *in*: R. Alkire and D. Kolb (Eds), 'Advances in Electrochemical Science and Engineering', vol. 8 (Wiley–VCH, Weiheim, 2003), p. 209.